REPORT

Reflectance and Color Variations on Mercury: Regolith Processes and Compositional Heterogeneity

Mark S. Robinson,[1]* Scott L. Murchie,[2] David T. Blewett,[2] Deborah L. Domingue,[2] S. Edward Hawkins III,[2] James W. Head,[3] Gregory M. Holsclaw,[4] William E. McClintock,[4] Timothy J. McCoy,[5] Ralph L. McNutt Jr.,[2] Louise M. Prockter,[2] Sean C. Solomon,[6] Thomas R. Watters[7]

Multispectral images of Mercury obtained by the MESSENGER spacecraft reveal that its surface has an overall relatively low reflectance with three large-scale units identified on the basis of reflectance and slope (0.4 to 1.0 micrometer). A higher-reflectance, relatively red material occurs as a distinct class of smooth plains that were likely emplaced volcanically; a lower-reflectance material with a lesser spectral slope may represent a distinct crustal component enriched in opaque minerals, possibly more common at depth. A spectrally intermediate terrain probably forms most of the upper crust. Three other spectrally distinct but spatially restricted units include fresh crater ejecta less affected by space weathering than other surface materials; high-reflectance deposits seen in some crater floors; and moderately high-reflectance, relatively reddish material associated with rimless depressions.

The MESSENGER spacecraft encountered Mercury on 14 January 2008, and the Mercury Dual Imaging System (MDIS) (*1*) acquired monochrome, 0.75-μm narrow-angle camera (NAC) and 11-color, 0.4- to 1.0-μm wide-angle camera (WAC) images of parts of Mercury never before seen by a spacecraft. We used WAC color observations (~5 km/pixel) in conjunction with NAC high-resolution (~200 to 500 m/pixel) monochrome images to explore the dominant sources of spectral heterogeneity on Mercury's surface and their correlation with morphologic features.

Early ground-based observations showed that Mercury had a low disk-integrated reflectance and a relatively featureless, positively sloping spectrum across the visible to near-infrared (near-IR) wavelengths (*2*). The lack of resolvable near-IR absorptions led to the conclusion that Mercury's surface is low in ferrous iron (*3*–*5*). Reflectance and mid-IR emission spectroscopy led to the hypothesis that Mercury's upper crust is predominantly composed of plagioclase feldspar, likely with lesser amounts of low-iron pyroxene (enstatite and diopside) and olivine (forsterite) (*4*, *6*, *7*). The surface of Mercury is expected to be heavily altered through space weathering processes that suppress absorption features, lower reflectance, and increase spectral slope (redden the spectrum), thus complicating interpretations of spectral data (*8*). Optically immature materials that are excavated as ejecta and rays from young craters are typically found in deposits less than 100 km in diameter. These smaller deposits contain the less-altered spectral signature of underlying rock and thus provide more definitive information about the composition of the crust and the nature of space weathering processes. The Mariner 10 spacecraft provided the first high-resolution panchromatic and color observations of Mercury (*3*). Similarly to the Moon, crater rays exhibited higher reflectance and shallower slope at visible wavelengths, indicating that space weathering processes operated on Mercury (*3*, *9*, *10*). A major surprise from the Mariner 10 multispectral observations was the lack of reflectance contrast between Mercury's smooth plains, which resemble lunar maria, and the adjacent terrain

[1]School of Earth and Space Exploration, Arizona State University, Tempe, AZ 85287, USA. [2]Johns Hopkins University Applied Physics Laboratory, Laurel, MD 20723, USA. [3]Department of Geological Sciences, Brown University, Providence, RI 02912, USA. [4]Laboratory for Atmospheric and Space Physics, University of Colorado, Boulder, CO 80303, USA. [5]National Museum of Natural History, Smithsonian Institution, Washington, DC 20560–0119, USA. [6]Department of Terrestrial Magnetism, Carnegie Institution of Washington, Washington DC, 20015, USA. [7]National Air and Space Museum, Smithsonian Institution, Washington, DC 20013, USA.

*To whom correspondence should be addressed. E-mail: robinson@ser.asu.edu

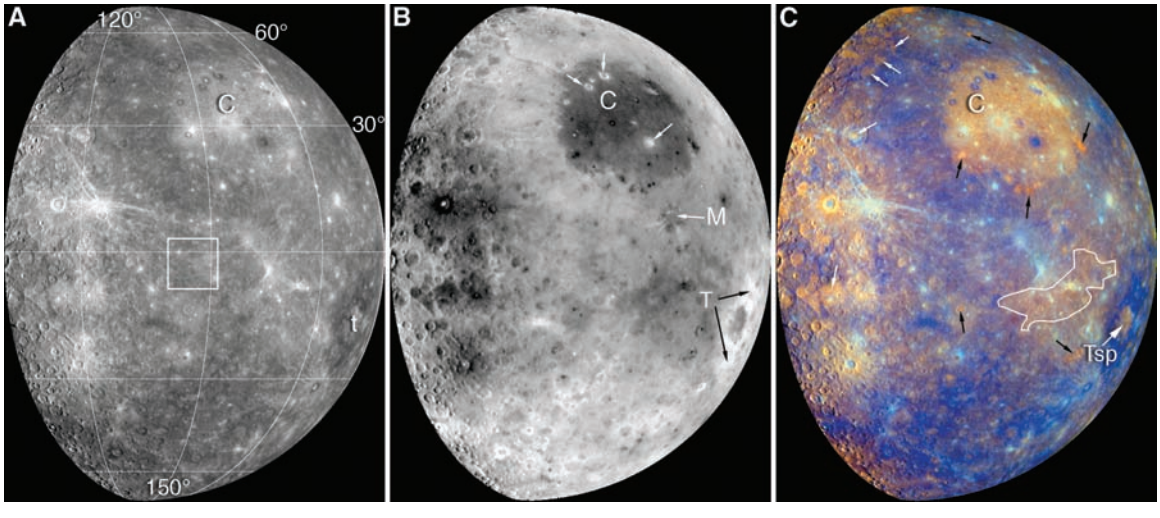

Fig. 1. MDIS WAC departure color sequence (EW0108829678 - EW0108829728C). (**A**) Photometrically corrected 560-nm-filter image. Largest reflectance contrasts are related to immature crater materials, the Caloris smooth plains (C), and Tolstoj basin (t) LRM. White box indicates standard spectral area used to normalize extracted spectra (Fig. 3A). (**B**) PC2 delimits regions with greatest color differences. Caloris smooth plains (C) and ejecta associated with Tolstoj basin (T) exhibit the greatest contrasts not associated with maturity variations. Low-reflectance craters (white arrows) in Caloris basin have the same high values in the PC2 image as Tolstoj ejecta (black arrows). (**C**) Color composite of spectral parameters used to separate units. Red is the inverse of PC2, green is PC1, and blue is relative visible color (430-nm/560-nm ratio). Unlabeled white arrows and irregular polygon indicate relatively young smooth plains deposits that exhibit clear spectral boundaries with basement materials (similar to Caloris plains, C), here interpreted to be volcanic in origin. Tsp denotes HRP within Tolstoj. Black arrows indicate red units interpreted as small volcanic centers.

(*3*, *9*, *10*). Initial analysis of color ratio images led to the conclusion that, unlike on the Moon, color units on Mercury are not well correlated with geomorphic units (*3*, *9*, *10*). Later work based on an improved radiometric calibration of the Mariner 10 color images indicated that at least a subset of smooth plains on Mercury do indeed correspond to color unit boundaries, which bolsters the hypothesis that some of the smooth plains deposits were emplaced as volcanic flows (*11*, *12*).

The MDIS image data (Figs. 1 and 2) were calibrated to radiance factor [known as reflectance, or I/F, observed radiance divided by solar irradiance from a normally solar-illuminated Lambertian disk (*13*)], map-projected, and photometrically corrected to standard viewing geometry (30° solar incidence and 0° emission angles) using a Hapke function with parameters (*14*) derived from Earth-based telescopic measurements. Principal component (PC) analysis was used to identify variations in the 11-band multispectral data set and to identify regions with like spectral properties. In this case, the first principal component (PC1) predominantly maps reflectance variations, whereas the second (PC2) discriminates color variations. Discrete reflectance boundaries in the PC2 map primarily correspond to morphologic boundaries and thus indicate variations in physical state or chemistry (Fig. 1B). To isolate color differences further, we computed color ratios and compared them with the PC maps. We determined distinct regions from these parameter maps (Fig. 1) and extracted representative spectra for analysis (Fig. 3).

MDIS revealed previously unimaged terrain whose reflectance and color properties are similar to those of the region imaged by Mariner 10 (*10*–*12*). The three areally dominant spectral units are low-reflectance material (LRM), moderate-to-high-reflectance smooth plains (HRP), and spectrally intermediate terrain (IT). The three units differ primarily in reflectance and share a red, lunar-like spectral slope indicative of mature, space-weathered soils. LRM (as much as ~30% lower than average reflectance) is widespread (Figs. 1 and 2); the most conspicuous exposures are found in the Tolstoj basin region (Fig. 2D), on some craters—most notably within the Caloris basin (Fig. 1, Fig. 2B)—and in the southern, heavily cratered parts of the newly imaged region (Fig. 1). In some instances, impact events excavated LRM from depth, and this material can be traced outward from the crater in the ejecta blanket (Fig. 2, C, E, and F). In all instances, the LRM has a moderate to shallow spectral slope (Fig. 3) and a shallow minimum near 600 nm. A broad annulus of somewhat dark material exterior to the Caloris basin is ~10% lower in reflectance than the planetary average, with complex interfingered IT and LRM occurrences. Several large craters within the Caloris basin are composed of LRM, indicating that a substantial portion of the material beneath the basin interior smooth plains is also LRM. This annulus of mixed material is approximately equivalent to previously mapped basin ejecta facies (*15*). However, crater counts for a portion of the annulus show that its age is less than that of the Caloris interior plains (*16*). HRP, exemplified by those plains that cover the floor of the Caloris basin, typically have reflectances ~10% above the hemispheric average and exhibit a slightly steeper (redder) spectral slope. Most of the heavily cratered terrain has reflectance properties intermediate to those between those of HRP and LRM.

Three other spectrally distinct but spatially restricted units are also recognized: fresh crater ejecta, bright crater-floor deposits (BCFDs), and moderately high-reflectance relatively reddish material (red spots) associated with rimless depressions. The immature crater ejecta are materials with reflectance elevated as much as 70% above IT and are associated with the walls, floors, and rays of young impact craters (Fig. 2A). These higher-reflectance materials also have a less-red spectral slope (Fig. 3), as do fresh lunar crater materials (*9*, *10*), suggesting that their optical properties have been less affected by space weathering. The BCFDs occur in distinct patches with abrupt boundaries and are found within only a few craters (Fig. 2B). Unlike fresh crater ejecta, the BCFD units do not appear to be associated with exposure of fresh material from the impact that formed the host crater. Similar bright floor deposits were identified in Mariner 10 images (*17*, *18*). This same material is also found in massifs of the peak rings of Raditladi and Eminescu basins. The peak-ring massifs are surrounded by aureoles of comparable high-reflectance material that extend radially for several kilometers. The red spots have elevated reflectances (up to 30% above average), occurring as diffuse halos surrounding scalloped-edged, rimless depressions along the margin of Caloris basin (*19*, *20*) and in the interiors of several craters of the southern heavily cratered terrain. These latter materials are distinguished from fresh-crater and BCFD materials by their spectral slope, which is the reddest observed by MESSENGER. Mariner 10 also observed materials with similar spectral characteristics, the most conspicuous found in the crater Lermontov (*10*, *11*, *18*), but central depressions were seen in only one (*10*).

A consistent attribute of spectra of all of the units is a lack of evidence for an absorption near 1-μm due to ferrous iron in silicates (Fig. 3A). WAC imaging has a spatial resolution two orders of magnitude higher than ground-based spectra, and it resolves fresh impact materials. To under-

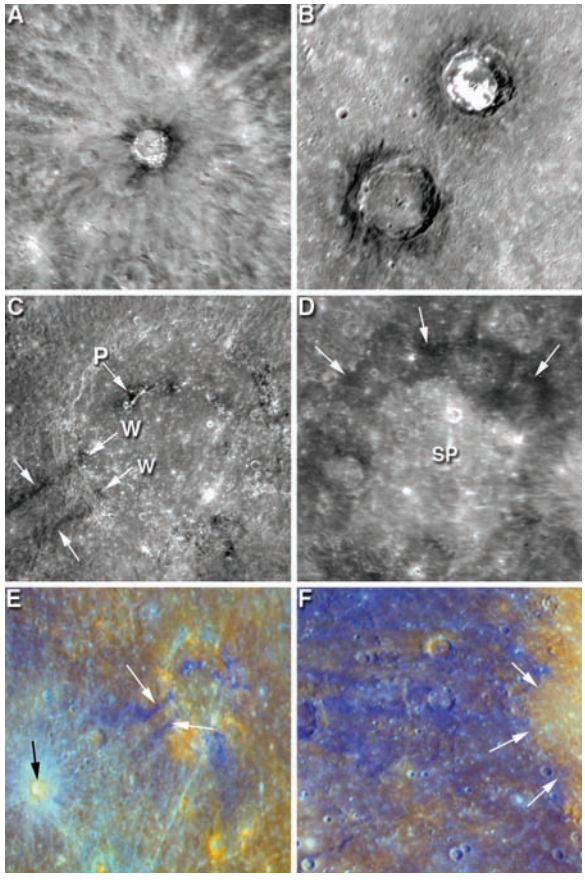

Fig. 2. (**A**) Basho crater (64-km diameter). High-reflectance ray material likely represents immature material, whereas the LRM near the rim may represent immature material of a different composition (EN0108828233M). (**B**) Two impact craters with low-reflectance walls found within the Caloris basin. Sander crater (upper right, 50-km diameter) exhibits BCFDs (EN0108826687M). (**C**) Linear streamers (unlabeled arrows) at Mozart crater (215-km diameter) trace LRM excavated during the impact. Exposures of the same material are visible in the crater wall (W arrows) and in the central peak ring (P) (EN0108827022M). (**D**) Tolstoj HRP (SP) superposed on LRM (arrows); image 825 km wide (EN0108828337M, EN0108828342M). (**E**) Color parameter image highlighting complex color relations. White arrows indicate color anomaly associated with LRM streamers at Mozart crater. Rayed crater at lower left illustrates common occurrence of redder material (black arrow) on the rim of immature craters; image ~800 km wide. (**F**) Western boundary of Caloris HRP (arrows) and basin rim. Note the radial color texture in the lower reflectance annular plains; image ~600 km wide [frame numbers and color scheme for (E) and (F) in Fig. 1 caption]. North is toward the top in all images.

stand the origin of Mercury's reflectance variations despite the low abundance of ferrous iron in silicate, it is informative to compare Mercury's reflectance to that of the Moon. Mercury's geometric reflectance is reported to range from 10% higher to 15% lower than the Moon (*14*), and recent estimates over a broad range of phase angles indicate that the Moon's reflectance is 7 to 17% higher than Mercury's, depending on phase angle (*21*). MESSENGER acquired low-resolution NAC (25 km/pixel) images of the Moon that provide a valuable reference for comparing with NAC Mercury images because the phase angle was nearly identical (65.8° for Mercury, 65.1° for the Moon), eliminating the need for photometric corrections. Comparison of two small areas (highlands on the Moon at 63.2°S, 275.8°E, and Mercury at 1.6°S, 116.1°E) at nearly identical photometric angles shows that Mercury's reflectance (mature IT) is ~27% lower than the mature lunar highlands area, with ~5 weight percent (wt %) FeO (*22*). Previous Moon-Mercury reflectance comparisons were tied to the lunar nearside. To perform a similar comparison, we normalized the Clementine 0.75-μm reflectance map of the Moon to 65° phase angle to match the I/F value at the standard location above, and we determined a lunar nearside average I/F of 0.022 (65° phase). This normalization depends only on the MDIS I/F values, removing uncertainties from the Clementine absolute radiometric calibration from our analysis. A similar approach was used to scale a photometrically normalized NAC 0.75-μm mosaic of the departing hemisphere of Mercury to 66° phase angle, revealing an average I/F of 0.019, a value 14 ± 3% lower than the lunar nearside average. These results are consistent with Earth-based estimates of I/F for the Moon and Mercury that show Mercury's I/F is 8% lower than that of the lunar nearside at 65° phase angle (V band 0.55 μm) (*21*).

Approximately one-third of the lunar nearside is covered by mare basalt containing 16 to 20 wt % FeO and 0 to 13 wt % TiO_2, compared with <6 wt % FeO and <1 wt % TiO_2 for the lunar highlands (*23*). In the absence of substantial iron in silicates, alternatives for lowering reflectance on Mercury include spectrally neutral opaque minerals (*10*) and meteoritic material (*24*). Both can provide a source of ferrous iron for space-weathering-produced submicroscopic metallic iron (known as SMFe or nanophase iron) blebs and coatings (*8*, *24*, *25*). Meteorite impacts are randomly distributed, so if meteoritic material were the source of ferrous iron, the surface of Mercury would be nearly uniform in reflectance except for rays of immature material. The major spectral trend in the data (Fig. 3) is caused by changes in slopes of both the visible and IR parts of the spectrum for fresh craters, consistent with exposure of immature regolith. However, a secondary trend in the data corresponds to a spectral change distinct from regolith maturity, from higher-reflectance smooth plains to LRM (Fig. 3B). This trend is especially evident at the Tolstoj basin. Tolstoj's interior smooth plains are relatively high in reflectance, whereas the ejecta deposits are relatively low in reflectance and less red. We interpret this distinct spectral trend to indicate that a low-reflectance, relatively spectrally neutral component occurs in the upper crust and is admixed in basin ejecta but absent in the smooth plains.

Supporting evidence for a low-reflectance component in portions of Mercury's crust comes from comparison of reflectances of fresh impact materials on Mercury and the Moon. If Mercury's bulk crust is predominantly composed of silicate minerals with low iron and titanium abundances (*4*, *6*, *7*, *9*, *10*), immature material should have relatively high reflectance, perhaps similar to or greater than immature materials found in the low-iron lunar farside highlands (*18*, *26*). Analysis of Mariner 10 images indicated that immature material on Mercury is up to 30% lower in reflectance than comparable immature lunar highland material (*18*). We find similar relations when comparing MDIS NAC mosaics of Mercury and Clementine 0.75-μm mosaics of the Moon, corrected to comparable phase angles as described above and resampled to 5 km/pixel. High-reflectance crater ejecta falls in the reflectance range 0.032 to 0.045 on Mercury, and 0.038 to 0.048 in the lunar highlands. Thus, the reflectance of immature material on Mercury is typically 10% to 20% lower than in the lunar highlands, indicating that Mercury's crust harbors a larger fraction of a low-reflectance component.

What is the nature of Mercury's low-reflectance component? The surface expression of LRM (Figs. 1A and 2) demands endogenic variations within the crust and is not simply an effect of space weathering. Low-reflectance halos interpreted as dark impact melt are observed at lunar craters such as Tycho (*27*), but there is no evidence that the production of impact glass alone could result in the reflectance contrast on the Moon or Mercury, and it is unlikely that the overall reflectance of a major regional unit such as the LRM can be attributed to impact melt. The spectral characteristics of the LRM (shallow visible to near-IR spectral slope and a shallow minimum near 600 nm) (Fig. 3B) are indicative of its composition. Opaque minerals such as ilmenite ($FeTiO_3$) and ülvospinel (Fe_2TiO_4) (*28*, *29*) are low in reflectance, have a flat spectral slope (spectrally neutral), and exhibit a minimum near 600 nm. Such minerals contain ferrous iron, but the 1-μm band is displayed as a broad, weak maximum. Mercury's low reflectance and overall red spectral slope requires that iron be present in some form (either ferrous or metallic or both). The presence of near-ultraviolet heterogeneity and the lack of an obvious 1-μm feature indicative of FeO in silicates are corroborated by the Mercury Atmospheric and Surface Composition Spectrometer (MASCS) surface reflectance spectra (*30*). The relatively flat spectral slope and the shallow minimum in normalized reflectance near 600 nm for

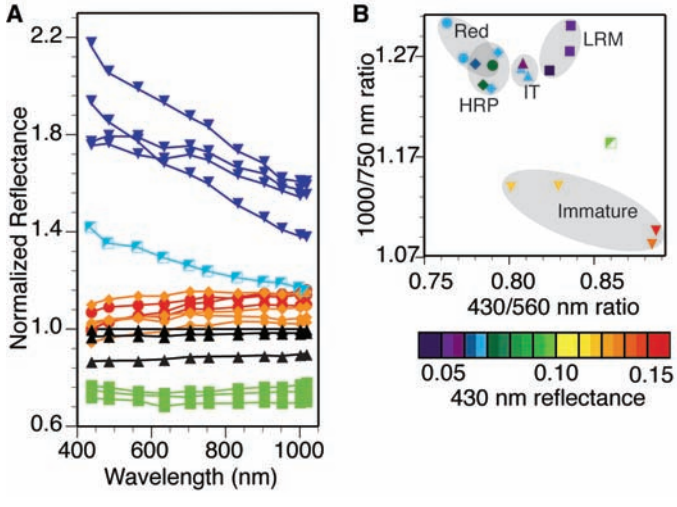

Fig. 3. (**A**) Spectral reflectance of key units discussed in the text, normalized to the standard area shown in Fig. 2A. Blue lines (downward-pointing triangles) are immature material, orange lines (diamonds) are smooth plains (HRP), red lines (circles) are red spots, solid black lines (upward-pointing triangles) are IT, lowest black line is the Caloris annular deposit, green lines (squares) are LRM, and the blue-green (half-filled squares) line is the BCFD found in Sander crater. (**B**) Key ratios used to distinguish spectral units; the single half-filled square corresponds to the Sander BCFD. The lower reflectance IT (diamond) corresponds to the Caloris low-reflectance annulus. The color scale codes the plotted points for absolute reflectance at 430 nm. The 1000-nm/750-nm ratio is a measure of spectral slope in the near-IR. Higher values indicate a steeper (redder) slope. The 430-nm/560-nm ratio is controlled by visible color. A higher value corresponds to a shallower visible slope; an upturn below ~500 nm also contributes to a higher value of this ratio. Generally, mature materials have steep slopes and hence plot in the upper left of the diagram, with immature materials (less steep) found in the lower right. Independent of the maturity trend, variations between major color units can be explained by a variable content of opaque material, which is dark and reduces the spectral slope.

the LRM are also seen in the MASCS data (*30*). From these observations and previous work (*2*–*7*, *10*, *18*, *21*), we propose that Mercury's crust is composed of iron-poor calcium-magnesium silicates (e.g., plagioclase, enstatite, pigeonite, and diopside) with a detectable component of spectrally neutral opaque minerals. Ilmenite ($FeTiO_3$) is the most likely candidate based on lunar analogy and cosmochemical abundance considerations. This lithology is broadly basaltic to gabbroic, with nearly all ferrous iron contained in opaque minerals and not in silicates, requiring redox conditions at or near the iron-wüstite buffer. An alternative to ilmenite is native iron metal, but such a material is relatively red at typical lunar regolith grain sizes (*29*, *31*) and implies more reducing conditions than iron-wüstite. The distinctively red smooth plains (HRP) appear to be large-scale volcanic deposits stratigraphically equivalent to the lunar maria (*20*), and their spectral properties (steeper spectral slope) are consistent with magma depleted in opaque materials. The large areal extent (>10^6 km^2) of the Caloris HRP is inconsistent with the hypothesis that volcanism was probably shallow and local (*10*); rather, such volcanism was likely a product of extensive partial melting of the upper mantle.

References and Notes

1. S. E. Hawkins III *et al.*, *Space Sci. Rev.* **131**, 247 (2007).
2. T. B. McCord, J. B. Adams, *Icarus* **17**, 585 (1972).
3. B. Hapke, G. E. Danielson Jr., K. Klaasen, L. Wilson, *J. Geophys. Res.* **80**, 2431 (1975).
4. J. Warell, *Icarus* **161**, 199 (2003).
5. F. Vilas, in *Mercury*, F. Vilas, C. R. Chapman, M. S. Mathews, Eds. (Univ. of Arizona Press, Tucson, 1988), pp. 59–76.
6. A. L. Sprague, T. L. Roush, *Icarus* **133**, 174 (1998).
7. J. Warell, D. T. Blewett, *Icarus* **168**, 257 (2004).
8. B. Hapke, *J. Geophys. Res.* **106**, 10039 (2001).
9. B. Hapke, C. Christman, B. Rava, J. Mosher, *Proc. Lunar Planet Sci. Conf.* **11**, 817 (1980).
10. B. Rava, B. Hapke, *Icarus* **71**, 397 (1987).
11. M. S. Robinson, P. G. Lucey, *Science* **275**, 197 (1997).
12. M. S. Robinson, G. J. Taylor, *Meteorit. Planet. Sci.* **36**, 841 (2001).
13. M. Minnaert, in *Planets and Satellites*, G. P. Kuiper, B. M. Middlehurst, Eds. (Univ. of Chicago Press, Chicago, 1961), pp. 213–248.
14. J. Veverka, P. Helfenstein, B. Hapke, J. D. Goguen, in *Mercury*, F. Vilas, C. R. Chapman, M. S. Matthews, Eds. (Univ. of Arizona Press, Tucson, 1988), pp. 37–58.
15. P. D. Spudis, J. E. Guest, in *Mercury*, F. Vilas, C. R. Chapman, M. S. Mathews, Eds. (Univ. Arizona Press, Tucson, 1988), pp. 118–164.
16. R. G. Strom *et al.*, *Science* **321**, 79 (2008).
17. D. Dzurisin, *Geophys. Res. Lett.* **4**, 383 (1977).
18. B. W. Denevi, M. S. Robinson, *Icarus*, in press 10.1016/j.icarus.2008.04.021 (2008).
19. J. W. Head *et al.*, *Science* **321**, 69 (2008).
20. S. L. Murchie *et al.*, *Science* **321**, 73 (2008).
21. J. Warell, *Icarus* **167**, 271 (2004).
22. P. G. Lucey, D. T. Blewett, B. L. Jolliff, *J. Geophys. Res.* **105**, 20297 (2000).
23. G. Heiken, D. T. Vaniman, B. M. French, *Lunar Sourcebook: A User's Guide to the Moon* (Cambridge Univ. Press, New York, 1991).
24. S. K. Noble, C. M. Pieters, *Sol. Syst. Res.* **37**, 31 (2003).
25. M. J. Cintala, *J. Geophys. Res.* **97**, 947 (1992).
26. D. T. Blewett, B. R. Hawke, P. G. Lucey, *Meteorit. Planet. Sci.* **37**, 1245 (2002).
27. B. R. Hawke, P. G. Lucey, J. F. Bell, R. Jaumann, G. Neukum, *Lunar Planet. Sci.* **17**, 999 (1986).
28. M. A. Riner, M. S. Robinson, J. A. Tangeman, R. C. Elphic, *Lunar Planet. Sci.* **36**, abstract 1943 (2005).
29. E. A. Cloutis et al., *Icarus*, in press; doi:10.1016/j.icarus.2008.04.018 (2008).
30. W. E. McClintock *et al.*, *Science* **321**, 62 (2008).
31. E. A. Cloutis, D. T. Bailey, M. A. Craig, P. S. Harderson, *Lunar Planet. Sci.* **39**, abstract 1082 (2008).

32. The hundreds of engineers and technical support personnel who brought MESSENGER from a concept to a successful flight project warrant the sustained appreciation of the mission science team. N. Laslo, H. Kang, R. Vaughan, A. Harch, R. Shelton, and A. Berman designed the imaging sequences that made this contribution possible. B. Denevi, K. Becker, and C. Hash are gratefully acknowledged for data calibration and processing. The MESSENGER project is supported by the NASA Discovery Program under contracts NAS5-97271 to Johns Hopkins University Applied Physics Laboratory and NASW-00002 to the Carnegie Institution of Washington.

6 May 2008; accepted 3 June 2008
10.1126/science.1160080

REPORT

Volcanism on Mercury: Evidence from the First MESSENGER Flyby

James W. Head,[1]* Scott L. Murchie,[2] Louise M. Prockter,[2] Mark S. Robinson,[3] Sean C. Solomon,[4] Robert G. Strom,[5] Clark R. Chapman,[6] Thomas R. Watters,[7] William E. McClintock,[8] David T. Blewett,[2] Jeffrey J. Gillis-Davis[9]

The origin of plains on Mercury, whether by volcanic flooding or impact ejecta ponding, has been controversial since the Mariner 10 flybys (1974–75). High-resolution images (down to 150 meters per pixel) obtained during the first MESSENGER flyby show evidence for volcanic vents around the Caloris basin inner margin and demonstrate that plains were emplaced sequentially inside and adjacent to numerous large impact craters, to thicknesses in excess of several kilometers. Radial graben and a floor-fractured crater may indicate intrusive activity. These observations, coupled with additional evidence from color images and impact crater size-frequency distributions, support a volcanic origin for several regions of plains and substantiate the important role of volcanism in the geological history of Mercury.

Volcanic deposits provide important clues to mantle composition, the location of past interior thermal anomalies, and the general thermal evolution of a planet. Relative to the other terrestrial planets, little is known with certainty concerning the history of volcanism on Mercury. In the more than three decades since Mariner 10 flew by Mercury in 1974–75, debate has persisted about the presence or absence of volcanic deposits (*1*), a question we address with data from the first flyby of Mercury by MESSENGER.

Whereas the Moon has distinctive composition-related differences in reflectance between highlands and volcanic maria, the reflectance of Mercury and of its smooth plains is relatively uniform, and therefore the role of volcanism is less obvious. Mariner 10 images, obtained shortly after the Apollo 16 mission to the Moon, revealed two widespread plains units that are similar to the lunar Cayley light plains (*2*, *3*): smooth plains and intercrater plains (*4*). These plains deposits on Mercury were interpreted to be volcanic in origin, on the basis of their smoothness and apparent ponding and embayment of lowland terrain (*4*, *5*). Other researchers, influenced by Apollo 16 results showing that similar-appearing deposits on the Moon were impact breccias, argued that Mercury's smooth plains represented basin ejecta deposits (*3*, *6*). The relatively low resolution of Mariner 10 images (typically ~1 km per pixel) was insufficient to resolve this issue. Lunar-like volcanic features, such as small shields, cones, sinuous rilles, and other vent-related structures, were not detected in Mariner 10 images (*7*, *8*), and the features that were observed did not provide conclusive evidence of a volcanic origin. For example, lobate fronts exposed at the edge of smooth plains suggested the presence of volcanic flow margins on Mercury, but similar features have been identified on the margins of lunar basin ejecta flows (*8*, *9*). The density of impact craters on Caloris

[1]Department of Geological Sciences, Brown University, Providence, RI 02912, USA. [2]Johns Hopkins University Applied Physics Laboratory, Laurel, MD 20723, USA. [3]School of Earth and Space Exploration, Arizona State University, Tempe, AZ 85287, USA. [4]Department of Terrestrial Magnetism, Carnegie Institution of Washington, Washington, DC 20015, USA. [5]Lunar and Planetary Laboratory, University of Arizona, Tucson, AZ 85721, USA. [6]Southwest Research Institute, 1050 Walnut Street, Boulder, CO 80302, USA. [7]Center for Earth and Planetary Studies, National Air and Space Museum, Smithsonian Institution, Washington, DC 20560, USA. [8]Laboratory for Atmospheric and Space Physics, University of Colorado, Boulder, CO 80303, USA. [9]Hawaii Institute of Geophysics and Planetology, University of Hawaii, Honolulu, HI 96822, USA.

*To whom correspondence should be addressed. E-mail: James_Head@brown.edu